PERGAMON

Acta mater. 48 (2000) 1383–1395

Acta MATERIALIA

www.elsevier.com/locate/actamat

BULK AMORPHOUS FC20 (Fe–C–Si) ALLOYS WITH SMALL AMOUNTS OF B AND THEIR CRYSTALLIZED STRUCTURE AND MECHANICAL PROPERTIES

A. INOUE† and X. M. WANG

Institute for Materials Research, Tohoku University, Sendai 980-8577, Japan

(Received 25 June 1999; accepted 16 September 1999)

Abstract—The addition of a small amount (0.4 mass%) of B to a commercial FC20 cast iron was found to cause the formation of an amorphous phase in melt-spun ribbon and cast cylinders with a diameter of up to 0.5 mm. The structure of a melt-spun B-free FC20 alloy consisted of α-Fe, γ-Fe and Fe_3C. The effectiveness of additional B is presumably due to the generation of attractive bonding nature among the constituent elements. The amorphous alloy ribbon exhibits a high tensile strength of 3480 MPa and good bending ductility. The annealing causes the formation of an amorphous phase containing α-Fe particles with a size of about 30 nm. The mixed phase alloy exhibits an improved tensile strength of 3800 MPa without detriment to good ductility. With further increasing temperature, the mixed amorphous and α-Fe structure changes to α-Fe + Fe_3C + graphite through the metastable structure of α-Fe + Fe_3C. The structure after annealing for 900 s at 1200 K has fine grain sizes of about 0.5 μm for α-Fe, 0.3 μm for Fe_3C and 1 μm for graphite. The graphite-containing alloy exhibits high tensile strength of 1200–2000 MPa and large elongation of 5–13%. The high tensile strength and good ductility were also obtained for the 0.5 mm cylinder annealed at 1200 K. The good mechanical properties are due to the combination of fine subdivision of crack initiation sites by the homogeneous dispersion of small graphite particles and the dispersion strengthening of Fe_3C particles against the deformation of the α-Fe phase. The synthesis of the finely mixed α-Fe + Fe_3C + graphite alloys having good mechanical properties by crystallization of the new amorphous alloy in the melt-spun ribbon and cast cylinder forms is encouraging for the future development of a new Fe-based high-strength and high-ductility material.

Keywords: Melt spinning; Transmission electron microscopy (TEM); Metallic glasses; Mechanical properties; Commercial cast iron

1. INTRODUCTION

It is well known that the structural change into an amorphous phase causes a drastic increase in mechanical strength [1, 2]. Recently, good mechanical properties have been obtained even for bulk amorphous alloys in the Zr–Al–Ni–Cu [3, 4], Zr–Ti–Al–Ni–Cu [4], Zr–Ti–Be–Ni–Cu [5] and Zr–M–Al–Ni–Cu (M = Nb or Pd) [6] systems and the combination of high static and dynamic strength and high fracture toughness has enabled us to use the bulk amorphous alloys as a new type of high-strength and high-toughness material [3, 4]. If Fe-based bulk amorphous alloys with high strength and good ductility are synthesized, an engineering value of the high-strength alloys is expected to increase drastically. It has been reported that Fe-based bulk amorphous alloys are produced in Fe–(Al, Ga)–(P, C, B, Si) [7, 8] and Fe–Co–(Zr, Nb)–(Mo, W)–B [9, 10] systems and the maximum diameter for glass formation is about 2 mm [9] for the former system and about 6 mm [10] for the latter system. However, no high tensile fracture strength exceeding 3000 MPa has been obtained for the Fe-based bulk amorphous alloys, because of their low ductility. It seems essential for the development of high strength Fe-based alloy to find a new alloy composition with higher glass-forming ability at more Fe-rich compositions. The shift of alloy composition to a more Fe-rich side is expected to result in the formation of an Fe-based amorphous alloy with good ductility. The increase in ductility also seems to cause an improvement of the annealing-induced embrittlement [11, 12] typical for Fe-based amorphous alloys. More recently, we have explored a new Fe-

† To whom all correspondence should be addressed.

1359-6454/00/$20.00
PII: S1359-6454(99)00394-8

based amorphous alloy with good bending ductility in as-quenched and crystallized states and found that commercial FC20 ($Fe_{81.1}C_{13.8}Si_{5.1}$ in at.%) alloys containing small amounts of B have good ductility in as-quenched and partially and fully crystallized states and exhibit high tensile strength of 3400 MPa for the as-quenched sample, 3800 MPa for the partially crystallized sample and 1500 MPa for the fully crystallized sample. It is noticed that the tensile strength level is 5–12 times higher than that for the FC20 alloy [13]. Furthermore, a bulk amorphous cylinder in the diameter range up to 0.5 mm is also formed in the FC20 alloys containing a small amount of B by copper mold casting. The aim of this paper is to present the B concentration range in which FC20 base amorphous alloys with good bending ductility are formed by melt spinning and copper mold casting and the compositional and annealing temperature dependence of the structure, tensile strength and ductility of the ductile FC20 base alloys, and to investigate the reasons for the high glass-forming ability and the appearance of the good mechanical properties.

2. EXPERIMENETAL PROCEDURE

A commercial FC20 cast iron defined by Japanese Industrial Standard (JIS) was used as a base alloy. The chemical alloy composition is shown in Table 1 in mass and atomic percentages. The FC20 alloys containing 0.3–2.0 mass% B were examined in the present study. Alloy ingots were prepared by induction melting commercial FC20 alloy and pure B crystal in an argon atmosphere. Rapidly solidified ribbons with a thickness of about 20 μm were produced by a melt spinning technique. Cylindrical bulk alloys with diameters up to 2 mm were also produced by a copper mold casting method. The amorphous structure was evaluated by means of X-ray diffraction and optical and transmission electron microscopy. Thermal stability was examined by differential scanning calorimetry at a heating rate of 0.33 K/s and the structural change upon crystallization was also examined by X-ray diffraction, optical microscopy, transmission electron microscopy and electron probe X-ray microanalysis. Mechanical properties of tensile strength, Young's modulus and elongation were measured with an Instron testing machine at a strain rate of 4.2×10^{-4}/s and at room temperature. Hardness was also measured with a Vickers microhardness tester under a load of 0.5 kN at room temperature.

Table 1. Chemical composition of a commercial FC20 cast iron

FC20	C	Si	Mn	P	S
Chemical composition (mass%)	3.42	2.93	0.21	0.095	0.015
Chemical composition (at.%)	13.77	5.05	0.18	0.15	0.02

The tensile fracture surface was examined by scanning electron microscopy.

3. RESULTS

3.1. Structure and mechanical properties of the as-quenched alloys

Figure 1 shows the X-ray diffraction patterns of the melt-spun FC20 alloys containing 0–2.0 mass% B. A drastic change in the X-ray diffraction pattern is seen between the 0 and 0.3 mass% B alloys. That is, the melt-spun structure consists of α-Fe, γ-Fe and Fe_3C for the 0 mass% B alloy and changes into an amorphous phase containing a small amount of α-Fe phase for the 0.3 mass% B alloy. In the higher B concentration alloys, no crystalline peak is seen, indicating the formation of an amorphous single phase. It is noticed that the addition of 0.4 mass% B enables us to form an amorphous single phase even for the FC20 alloy. The absence of an amorphous phase in the FC20 cast iron corresponding to $Fe_{81.1}C_{13.8}Si_{5.1}$ (at.%) is consistent with the previous data [14] on the composition ranges of amorphous alloys in Fe–metalloid systems. Figure 2 shows the differential DSC curves of the melt-spun FC20 alloys containing 0.3–2.0 mass% B. Two distinct exothermic peaks marked with T_{p1} and T_{p2} are seen, indicating that the amorphous phase crystallizes through multiple stages. The onset and peak temperatures of the first exothermic peak increase gradually from 775 to 813 K and from 786 to 823 K, respectively, with increasing B content. In addition to the exothermic peaks, one can see a weak endothermic peak corresponding to the Curie temperature as marked with T_c and the Curie temperature also increases from 643 to 658 K with increasing B content to 2.0 mass%.

The changes in the Young's modulus (E), tensile fracture strength (σ_f) and Vickers hardness (H_v) with B content were examined for the FC20 alloys containing 0.3–2.0 mass% B. All the properties increase gradually with increasing B content, i.e. from 122 to 132 GPa for E, from 3400 to 3680 MPa for σ_f and from 950 to 1110 for H_v. The increases in all the properties indicate that the bonding nature among the constituent elements becomes strong by the addition of B. We also examined the stability of the mechanical properties of the Fe-based amorphous alloys against annealing embrittlement before crystallization. Figure 3 shows the changes in the E, σ_f and H_v as a function of annealing temperature (T_a) for the melt-spun FC20 alloy containing 0.4 mass% B. The T_a lies well below T_x (780 K). The E, σ_f and H_v are 125 GPa, 3480 MPa and 970, respectively, in the as-quenched state, increase gradually with increasing T_a, show a maximum of 135 GPa, 3850 MPa and 1120, respectively, at $T_a = 680$ K and then decrease with further increasing T_a to 740 K. Considering the annealing

time for 900 s, the annealing at 740 K appears to correspond to an incipient stage of crystallization. Consequently, the amorphous FC20 alloy containing 0.4 mass% B can keep good ductility and shows improved mechanical properties in the annealed state. It is noticed that no distinct annealing-induced embrittlement is recognized. This behavior is in good contrast with the previously reported result [2] that annealing at temperatures well below T_x causes the catastrophic loss of ductility for Fe-based amorphous alloys in Fe–P and Fe–B binary and Fe–P–C, Fe–P–B, Fe–Si–B and Fe–B–C ternary systems.

3.2. Changes in the structure and mechanical properties upon crystallization

Figure 4 shows the X-ray diffraction patterns of the amorphous FC20 alloy containing 0.4 mass% B after annealing for 900 s at various temperatures between 680 and 1200 K. No diffraction peak due to a crystalline phase is seen in the as-quenched

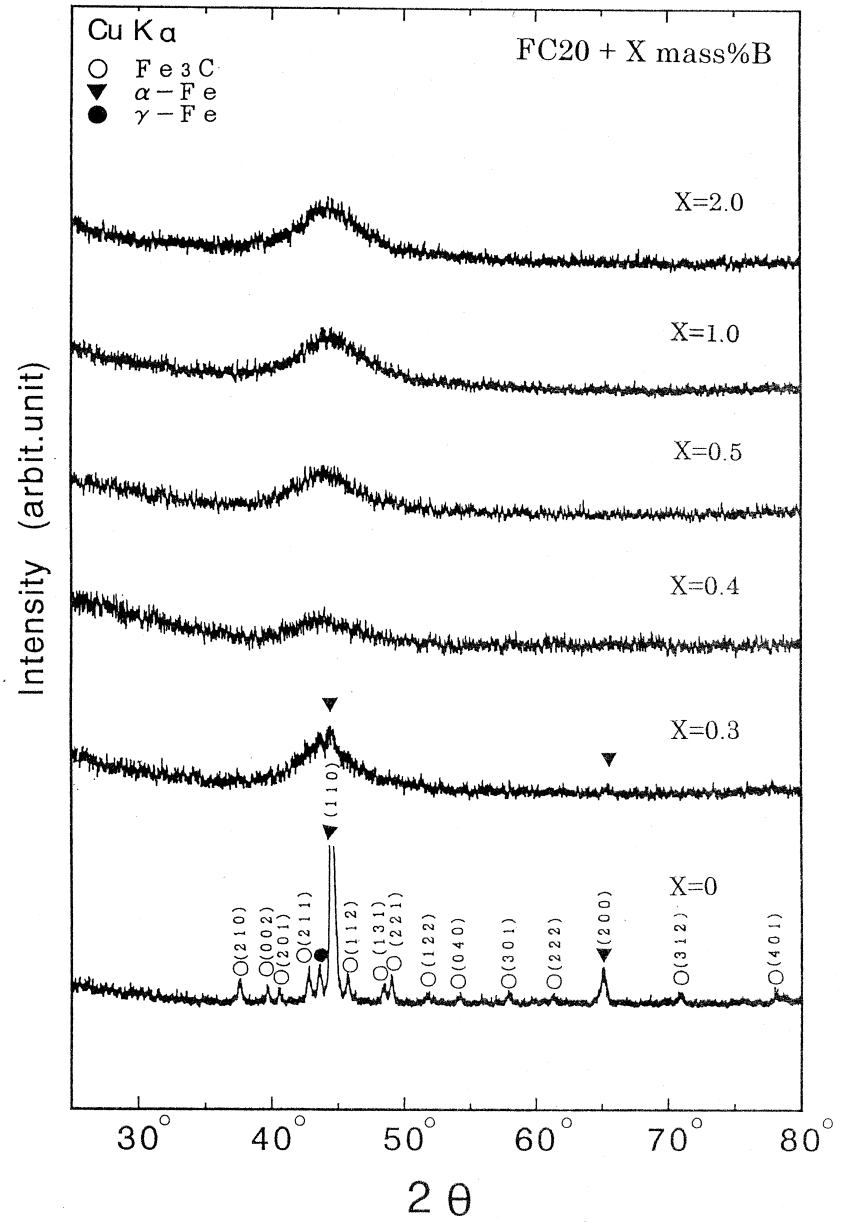

Fig. 1. X-ray diffraction patterns of melt-spun FC20 alloys containing various B contents ranging from 0 to 2.0 mass% B.

state, but a weak diffraction peak of α-Fe is recognized for the sample annealed at 680 K. The diffraction peak of α-Fe becomes distinct by an increase in T_a to 810 K. With an increase in T_a to 850 K, extra peaks of Fe_3C are distinctly seen. However, the peak intensity of Fe_3C appears to decrease for the alloy annealed at 1200 K, indicating the decrease in the precipitation amount of Fe_3C phase. The structure of the commercial FC20 alloy consists of α-Fe and graphite. Therefore, the present FC20 alloy containing 0.4 mass% B is expected to contain graphite, though the identification of the graphite phase by X-ray diffraction is difficult. From the X-ray diffraction patterns of the FC20 amorphous alloys containing 0.3–2.0 mass% B annealed for 900 s at 1200 K, the structure is identified to consist of α-Fe and Fe_3C for the 0.3 and 0.4 mass% B alloys and α-Fe, Fe_3C and Fe_3Si for the 0.5, 1.0 and 2.0 mass% B alloys. We tried to confirm the precipitation of graphite and to clarify the particle size and interparticle spacing of the graphite. Figure 5 shows a scanning electron micrograph taken from the surface of the sample annealed for 900 s at 1200 K. Nearly spherical particles with dark contrast disperse homogeneously and the particle size and interparticle spacing are about 0.5–1.5 μm and 0.5–2 μm, respectively. The alloy components in the dark contrast region and the matrix region with the bright contrast were examined by energy dispersive X-ray spectroscopy. From the ordinary secondary electron image and electron probe X-ray images of Fe, B and C elements, it has

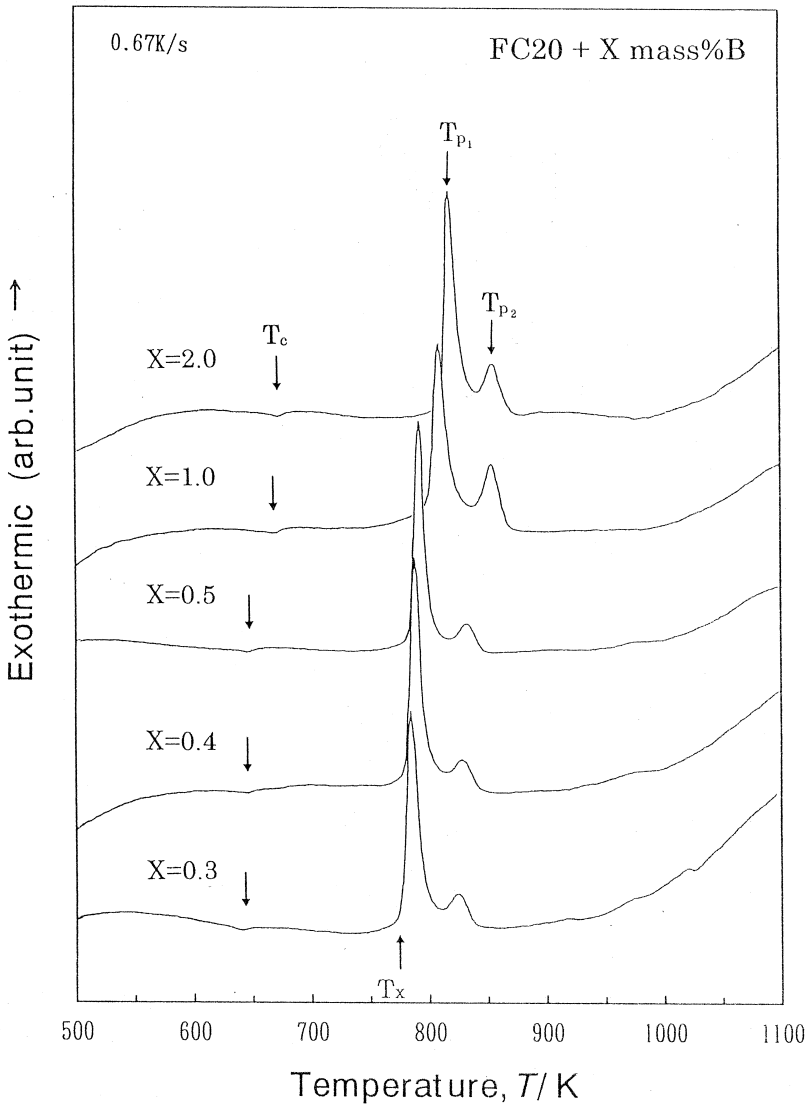

Fig. 2. Differential scanning calorimetric curves of the melt-spun FC20 alloys containing various B contents.

been confirmed that the matrix phase is mainly composed of Fe and the spherical dark contrast particles correspond to graphite. No appreciable segregation of B is recognized. In order to confirm the precipitation of graphite particles, TEM observation was performed for the crystallized sample. Figure 6 shows a bright-field electron micrograph (a) and selected-area electron diffraction patterns (b–d) of the sample annealed for 900 s at 1200 K. The diffraction pattern (d) taken from the flower-like contrast D region consists of some diffraction rings which are identified as hexagonal graphite. The ring pattern also indicates that the graphite is composed of fine grains with random orientations. The diffraction patterns (b) and (c) taken from regions B and C, respectively, are identified to be b.c.c. α-Fe and orthorhombic Fe_3C phases, respectively. It is confirmed that the matrix phase is composed of α-Fe with a size of about 0.5 μm and Fe_3C with a size of about 0.3 μm. Thus, the three constituent phases have fine grains. In comparison with the grain sizes of α-Fe and graphite in the conventional FC20 cast iron, their grain sizes for the present alloy are smaller by three to four orders of magnitude. Considering that conventional plain carbon steels and gray cast irons are composed of α-Fe, Fe_3C, graphite, γ-Fe and martensite and do not include any other compounds including $Fe_3(Si, B)$ phase, the subsequent study was focused on the FC20 alloy containing 0.4 mass% B in which the $Fe_3(Si, B)$ phase is absent. The 0.4 mass% B is a minimum B concentration for the formation of an amorphous single phase.

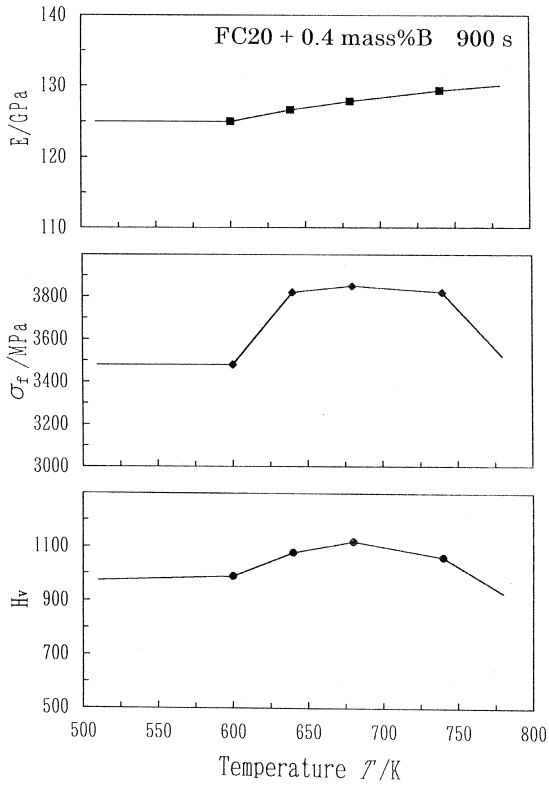

Fig. 3. Changes in the Young's modulus (E), tensile fracture strength (σ_f) and Vickers hardness (H_v) with annealing temperature (T_a) for 900 s for the melt-spun FC20 alloy containing 0.4 mass% B.

We have already demonstrated that the amorphous FC20 alloy containing 0.4 mass% B keeps good bending ductility even after annealing at the temperature just below T_x. In addition, it was found that the 0.4 mass% B alloy exhibits again good bending ductility in a crystallized state where T_a is above 850 K. Figure 7 shows the changes in the tensile fracture strength (σ_f), fracture elongation (ε_f) and Vickers hardness (H_v) with annealing temperature for 900 s, together with the data of the DSC curve and the crystallized structure. The alloy crystallizes through the process of $Am \rightarrow Am' + \alpha\text{-}Fe \rightarrow Am'' + \alpha\text{-}Fe + Fe_3C \rightarrow \alpha\text{-}Fe + Fe_3C \rightarrow \alpha\text{-}Fe + Fe_3C +$ graphite. As is evident from the comparison with the data on bending ductility, the mixed phase alloys of $Am'' + \alpha\text{-}Fe + Fe_3C$ and $\alpha\text{-}Fe + Fe_3C$ are brittle and the other structure alloys have good bending ductility. The maximum tensile strength of 3900 MPa is obtained in the amorphous phase state containing nanoscale α-Fe particles. The further progress of crystallization accompanying the precipitation of Fe_3C as well as the disappearance of the remaining amorphous phase leads to a significant decrease in tensile strength, while the elongation increases significantly in the annealing temperature range above 1000 K. It is noticed that the alloy annealed at 1200 K has large elongation of 11% combined with high tensile fracture strength of 1480 MPa. The large elongation for the melt-spun ribbon of 20 μm in thickness indicates that the annealed alloy is extremely ductile. Figure 8 shows the fracture surface appearance of the as-quenched and annealed (680 and 1200 K) samples. There is a distinct difference in the fracture surfaces. The fracture of the alloys containing the amorphous phase takes place along the maximum shear plane that is declined by about 45 deg to the direction of tensile load. The fracture surface of the as-quenched amorphous alloy consists of typical smooth and vein patterns caused by shear sliding and final instantaneous fracture, respectively. A similar feature is also recognized for the sample annealed at 680 K, but the area occupied by the smooth region decreases and the density of the vein increases. The dispersion of nanoscale α-Fe particles causes the suppression of the shear sliding as well as the increase in the number of crack nucleation sites at the final fracture stage. The fully crystallized alloy reveals a dimple pattern typical of ductile metallic crystalline alloys in which a number of crack initiation sites are homogeneously dispersed.

3.3. Preparation of cast bulk cylinders with high tensile strength and large elongation

As described above, the addition of a small amount of B (0.4 mass% B) to commercial FC20 alloy causes the formation of the amorphous single phase with high tensile strength of 3800 MPa. Furthermore, the fully crystallized alloy consists of a fine mixture of α-Fe, Fe_3C and graphite and exhibits good mechanical properties of tensile strength of 1300 MPa combined with large elongation of about 13%. The strength of the crystallized alloy is about six to seven times higher than that for the FC20 cast iron. Although a number of studies on the microstructure and mechanical properties for Fe-based amorphous alloys subjected to crystallization treatment were performed up to date, there have been no data on the simultaneous achievements of high strength and large elongation for Fe-based alloys obtained by crystallization of an amorphous phase. The first achievement of good mechanical properties in the crystalline state for Fe-based amorphous alloys gives us a unique opportunity to examine the dependence of the as-cast structure for the good mechanical properties and to clarify the possibility of synthesizing a bulk Fe-

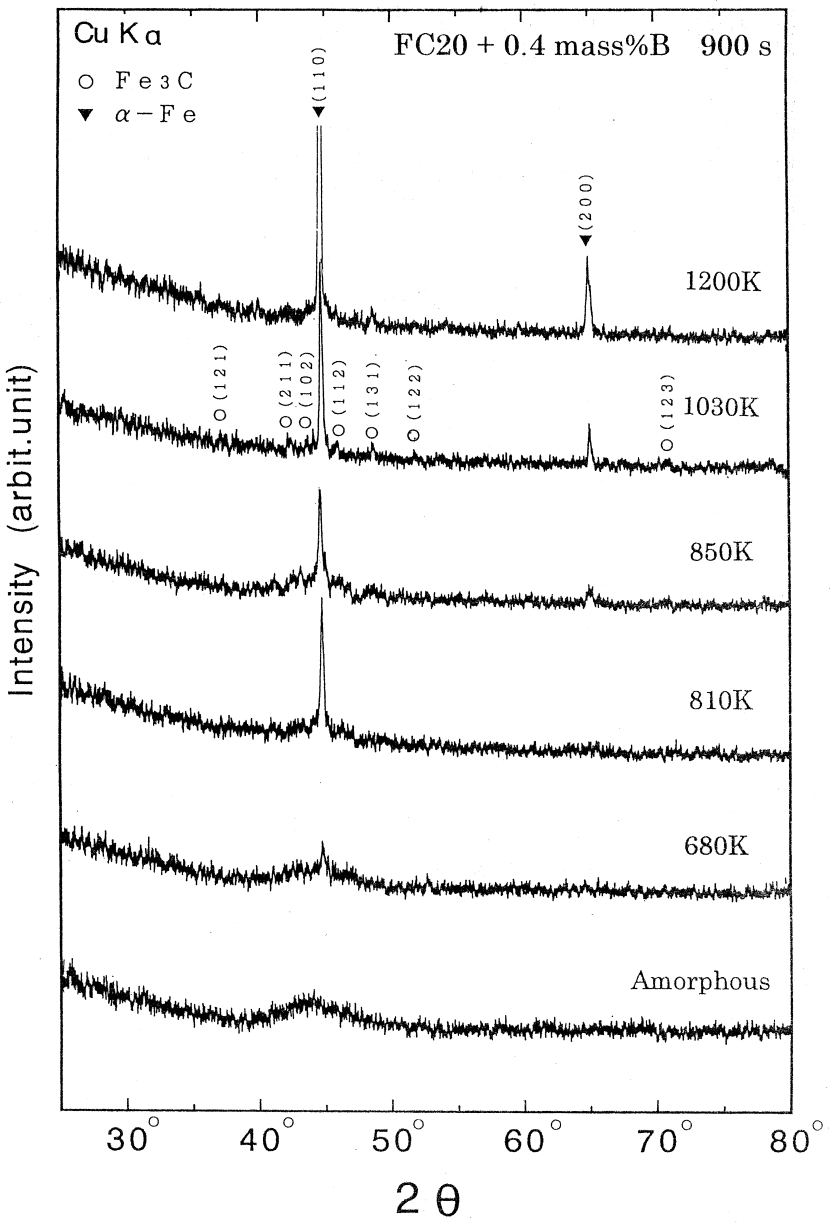

Fig. 4. X-ray diffraction patterns of the melt-spun FC20 + 0.4 mass% B alloy annealed for 900 s at various temperatures between 680 and 1200 K.

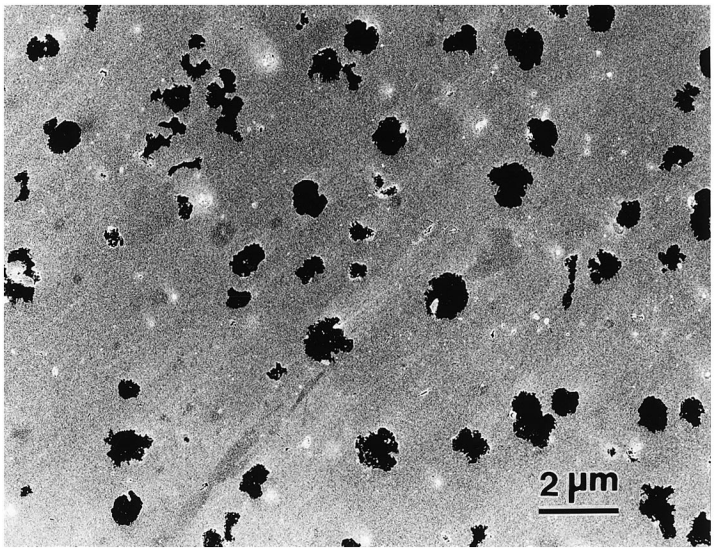

Fig. 5. Scanning electron micrograph of the melt-spun FC20 + 0.4 mass% B alloy annealed for 900 s at 1200 K.

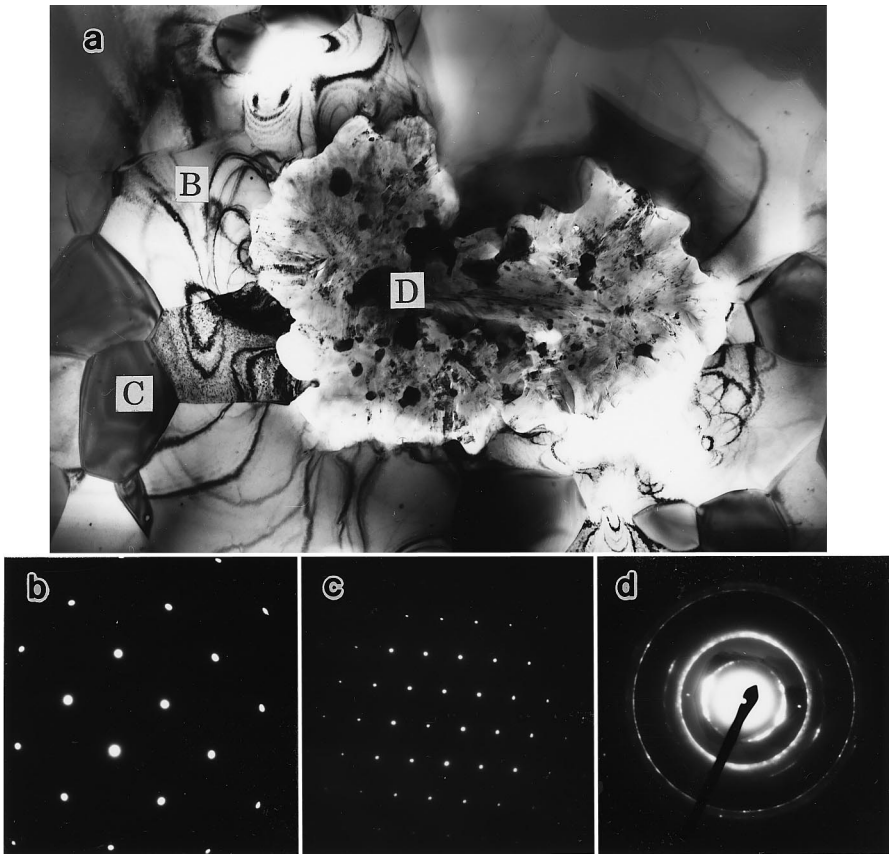

Fig. 6. Bright-field electron micrograph (a) and selected-area electron diffraction patterns (b)–(d) taken from regions B, C and D, respectively, in (a) for the melt-spun FC20 + 0.4 mass% B alloy annealed for 900 s at 1200 K.

based alloy with high strength and large elongation by the casting and annealing process. Figure 9(a) shows an outer surface appearance of the FC20 alloy containing 0.4 mass% B with a diameter of 0.5 mm prepared by the copper mold casting method. The outer surface is rather smooth and no distinct raggedness due to the precipitation of a crystalline phase is seen. Figures 9(b) and (c) show an X-ray diffraction pattern and an optical micrograph taken from the outer surface of the transverse cross section for the cast cylinder with a diameter of 0.5 mm, respectively. No distinct contrast revealing the precipitation of a crystalline phase is seen over the whole cross section and the X-ray diffraction pattern consists mainly of a broad peak due to the formation of an amorphous phase. These metallographic data indicate that the cast cylinder is mainly composed of an amorphous phase. Furthermore, in the optical micrographs of the cylinder with a diameter of 0.5 mm annealed for 900 s at 1200 K, we have observed a high density of nearly spherical dark contrast regions of about 1 μm in diameter corresponding to a graphite phase. Considering that the X-ray diffraction pattern of the annealed cylinder consists of α-Fe and Fe_3C phases, the matrix phase is concluded to be occupied by the two phases. There is no appreciable difference in the morphology and size of the graphite phase between the melt-spun ribbon and the cast cylinder, and hence the α-Fe and Fe_3C phases seem to keep fine grain sizes of about 0.5 and 0.3 μm, re-

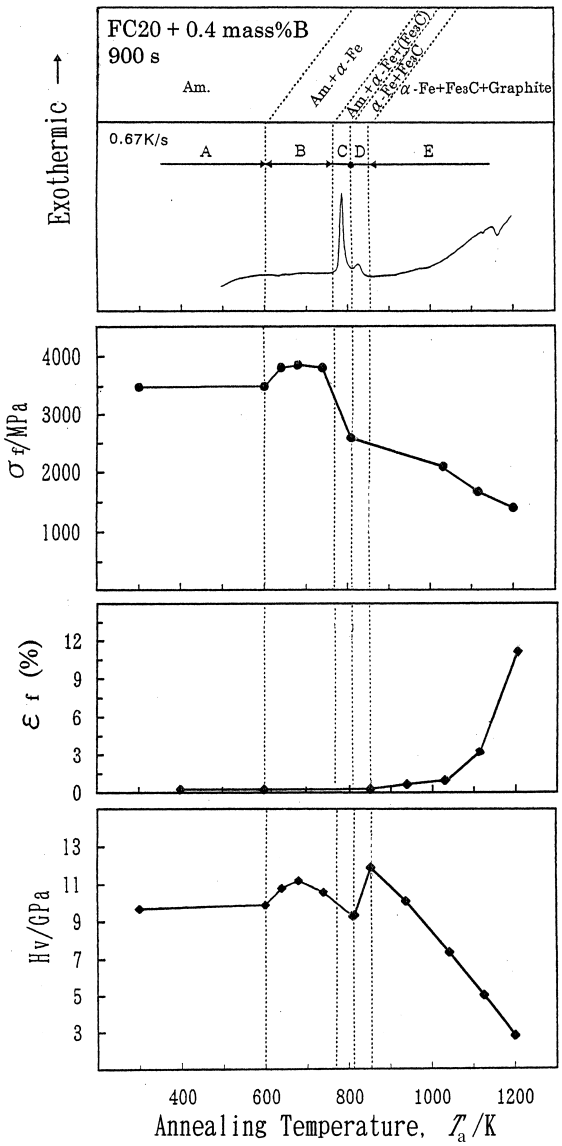

Fig. 7. σ_f, ε_f and H_v as a function of T_a for the melt-spun FC20 + 0.4 mass% B alloy. The annealing time is 900 s. The data on the DSC curve and structural change are also shown for reference.

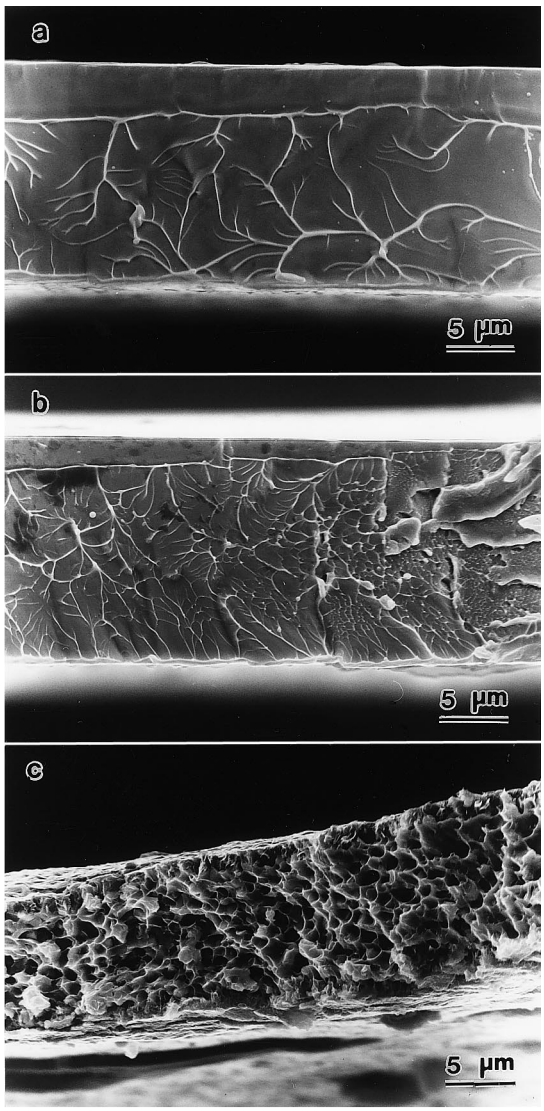

Fig. 8. Scanning electron micrographs of the tensile fracture surface of the melt-spun FC20 + 0.4 mass% B alloy: (a) as-quenched; (b) annealed for 900 s at 680 K; (c) annealed for 900 s at 1200 K.

spectively, which are the same as those for the melt-spun ribbon.

We further examined the tensile fracture strength and elongation for the cast amorphous FC20 + 0.4 mass% B cylinders annealed for different periods at 1200 K. Figure 10 shows the tensile stress–elongation curve of the 0.5 mm cylinder with the mixed structure of α-Fe, Fe_3C and graphite phases obtained by annealing for 3.6 ks. The 0.2% proof strength, tensile fracture strength and elongation are 1420 MPa, 1530 MPa and 9%, respectively, after 3.6 ks, indicating that the annealed alloy has high tensile strength combined with high ductility. These mechanical characteristics are nearly the same as those for the annealed ribbon samples. The tensile fracture surface also consists of a well-developed dimple pattern in which the initiation of tensile cracks appears to occur in the graphite region with a size of about 1 μm, as shown in Fig. 11. The size of each dimple agrees with that of the graphite particles and hence the homogeneous dispersion of the fine graphite particles is recognized to contribute to the achievement of the good mechanical properties. Furthermore, the Vickers hardness numbers in as-cast and annealed states were 970 and 285, respectively, for the 0.5 mm cylinder and 980 and 310, respectively, for the 1 mm cylinder. These hardness numbers are nearly the same as those for the melt-spun ribbon, indicating the absence of a distinct difference in mechanical properties between

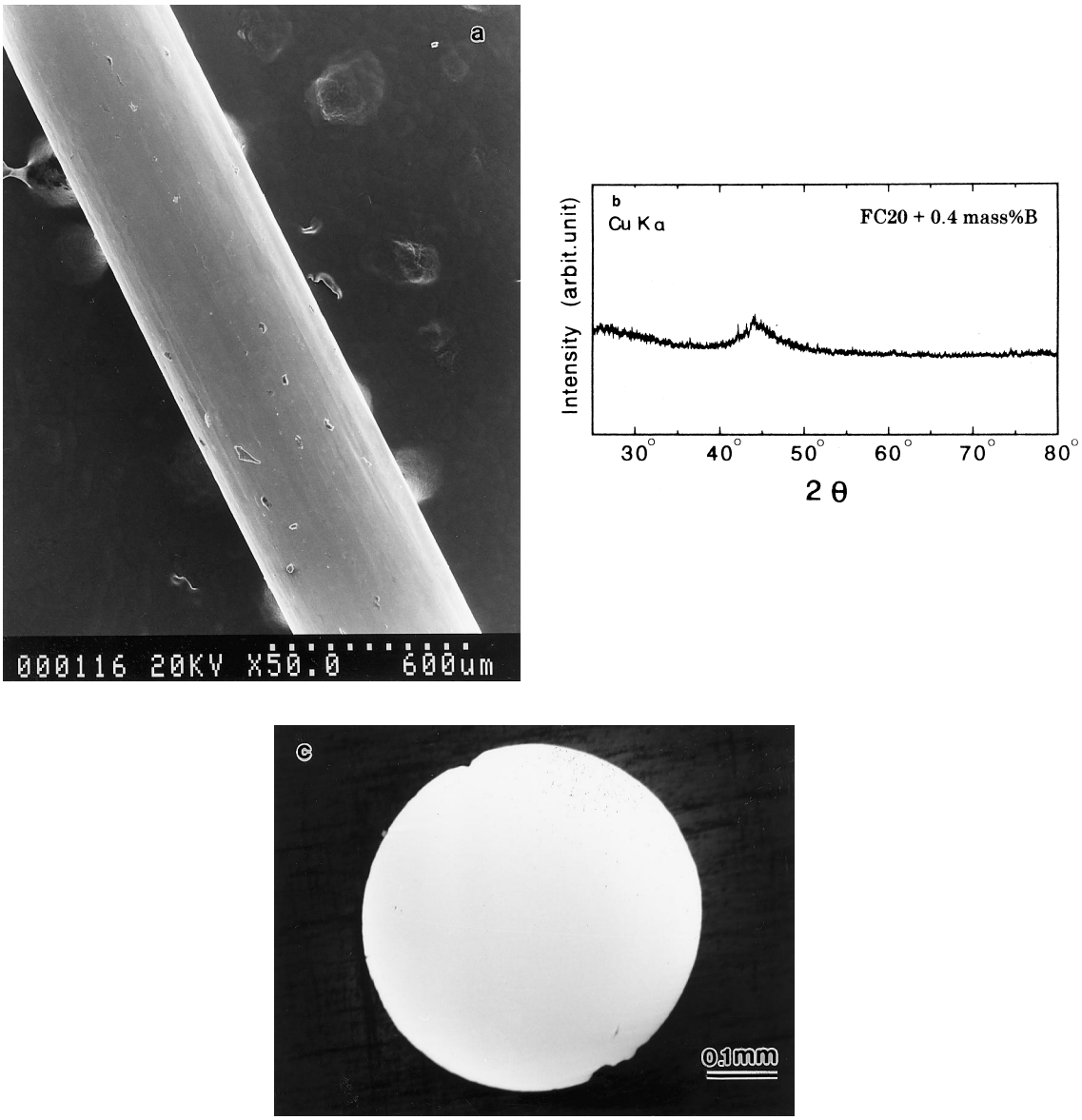

Fig. 9. Scanning electron micrograph of the outer surface (a), X-ray diffraction pattern (b) and optical micrograph of the transverse cross-section (c) and X-ray diffraction pattern (c) of a cylindrical FC20 + 0.4 mass% B rod with a diameter of 0.5 mm produced by the copper mold casting process.

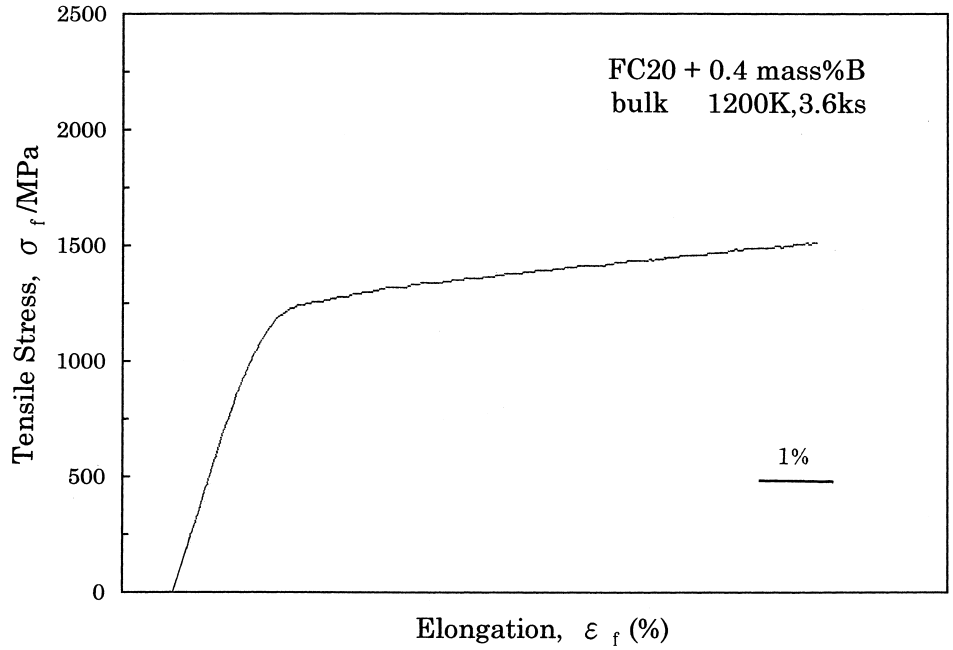

Fig. 10. Tensile stress–elongation curve of the cast amorphous FC20 + 0.4 mass% B cylinder of 0.5 mm in diameter annealed for 3.6 ks at 1200 K.

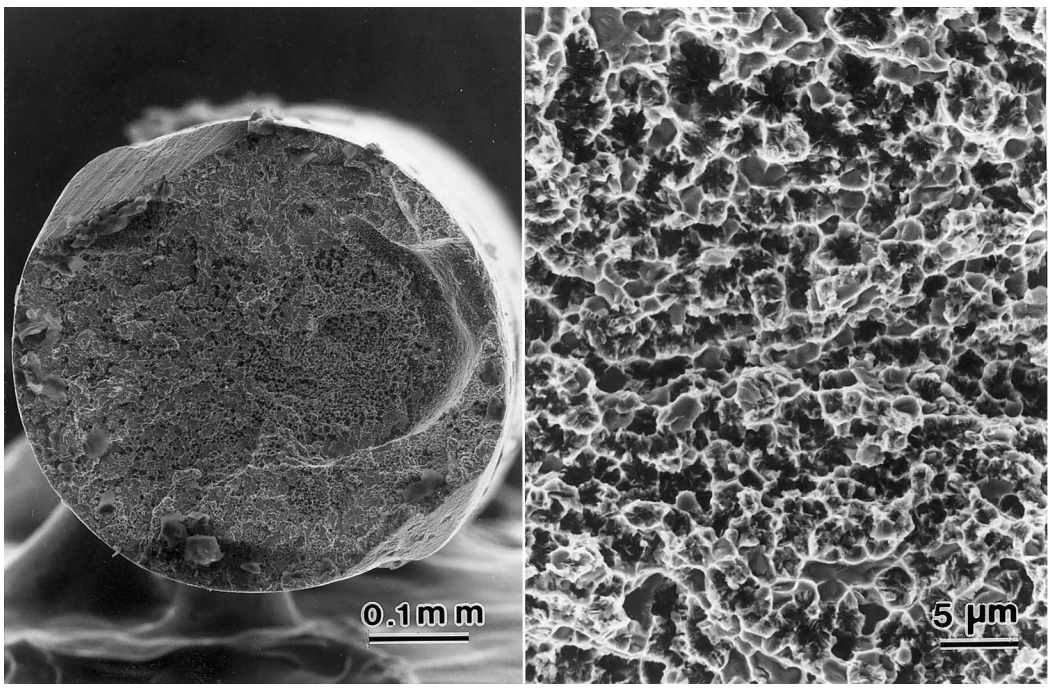

Fig. 11. Tensile fracture surface appearance of the cast amorphous FC20 + 0.4 mass% B cylinder of 0.5 mm in diameter annealed for 3.6 ks at 1200 K.

the cast cylinders and the melt-spun ribbon. The annealed cylinders of 0.5 and 1 mm in diameter can be significantly bent into ring forms at room temperature. The good cold workability is consistent with the large elongation resulting from the finely mixed structure for the annealed alloy.

4. DISCUSSION

4.1. Effectiveness of the addition of a small amount of B on the amorphous phase formation

The chemical compositions of the commercial FC20 alloy shown in Table 1 imply that the FC20 cast iron and the FC20 alloy containing 0.4 mass% B have atomic compositions of $Fe_{81.1}C_{13.8}Si_{5.1}$ and $Fe_{80.4}C_{13.7}Si_{4.3}B_{1.6}$, respectively. As shown in Fig. 1, the melt-spun structure consists of α-Fe + γ-Fe + Fe_3C phases for the former alloy and an amorphous phase for the latter alloy. The drastic change indicates the effectiveness of the 1.6 at.% B addition on the formation of the amorphous phase. It is well known that no amorphous phase is formed in Fe–C binary and Fe–C–Si ternary alloys by melt spinning, though an amorphous phase is formed in the region near the hole in the thin foil prepared by the gun or piston-anvil techniques [15]. The as-quenched structure of the melt-spun Fe–C–Si alloy is consistent with a number of previous data [15, 16]. The increase in the glass-forming ability has been achieved by the satisfaction of the three empirical rules for the stability of supercooled liquid [3, 17], i.e. (1) multi-components consisting of more than three elements, (2) significant difference in atomic size ratios above about 12%, and (3) suitable negative heats of mixing. Based on the three empirical rules, the poor glass-forming ability of the Fe–C and Fe–C–Si alloys is attributed to the non-satisfaction of the third factor because the main Fe–C pair has a positive heat of mixing. Consequently, it is easily expected that the addition of an element leading to the satisfaction of the third factor is effective for the improvement of glass-forming ability. We paid attention to the B element because B addition causes a more continuous change in atomic size of Fe > Si > C > B and the generation of strongly negative bonding pairs of Fe–B, C–B and Si–B. The coexistence of these atomic pairs decreases the atomic diffusivity and increases the viscosity of the supercooled liquid, leading to the increase in thermal stability against crystallization. The weak bonding nature is also supported from the precipitation of a high volume fraction of graphite and the absence of Fe_3C for the Fe–C–Si ternary alloy. On the other hand, the addition of 1.2–1.6 at.% B (0.3–0.4 mass% B) causes the precipitation of Fe_3C. The formation of Fe_3C is due to the increase in the phase stability by the dissolution of B into Fe_3C [18]. The dramatic influence of B is also supported by the result that an $Fe_3(Si, B)$ [18] phase is formed for the 2.0 at.% B-containing alloy. The 1.6 at.% B is said to be the lowest content for the satisfaction of the general rules in which the fully crystallized structure from an amorphous phase in metallic base systems always contains more than one kind of compound.

4.2. Increase in the tensile strength for the Fe–C–Si–B amorphous alloy containing nanoscale α-Fe particles

There have been a number of data on the embrittlement of Fe-based amorphous alloys upon annealing at temperatures well below crystallization temperature [11, 12]. No exceptional example for the annealing-induced embrittlement has been reported for typical Fe–metalloid and Fe–metal type amorphous alloys containing more than 70 at.% Fe. On the other hand, it has recently been found [19] that the homogeneous dispersion of nanoscale metallic particles into an amorphous matrix in Al-, Mg-, Ni- and Fe–Ni-based systems by partial crystallization of the amorphous phase causes an increase in tensile strength by about 1.4 times without detriment to ductility. More recently, the simultaneous increases in tensile strength and elongation have also been reported in the nanoscale mixed structure consisting of amorphous and Zr_2Cu particles [20]. The present annealed, 0.4 mass% B, Fe-based alloy consists of amorphous matrix containing α-Fe particles with a size of about 30 nm. The α-Fe particles have very low solute concentrations and hence the precipitation of the nanoscale α-Fe particles causes the enrichment of solute elements into the remaining amorphous matrix. In the nanoscale mixed structure, the key point whether or not the mixed phase alloys exhibit good ductility and high tensile strength is attributed to the ductility of the remaining amorphous phase. As described above, the main solute elements of C and Si cannot make any kind of compound in the $Fe_{82}C_{13.7}Si_{4.3}$ alloy. This indicates that the bonding nature among the constituent elements in the Fe–C–Si–B alloy is not in a strong state and hence the rather weak bonding enables the maintenance of good ductility even after the enrichment of solute elements into the remaining amorphous phase. The presumption that the bonding among the constituent elements is rather weak even for the Fe–C–Si–B alloy is supported by the precipitation of graphite in α-Fe and Fe_3C phases.

Furthermore, the increase in the tensile strength and Vickers hardness by the precipitation of the nanoscale α-Fe particles is presumed to result from the combination of (1) high strength of α-Fe particles due to the perfect crystal effect. That is, the α-Fe particles are too small to contain dislocations. (2) The suppression of cracks along the interface between the amorphous matrix and nanoscale par-

ticles. This is induced by the formation of a higher degree of dense packed interface structure resulting from the lower interfacial energy at the amorphous/crystal interface as compared with the crystal/crystal interface energy [21]. (3) The suppression of shear sliding of the amorphous matrix by the homogeneous dispersion of the nanoscale α-Fe particles with a size of about 30 nm which is comparable with the thickness (20–30 nm) [22] of the shear deformation band for the amorphous alloys. The strengthening mechanism seems to be the same as those [16] for the previously reported Al-, Mg- and Ni-based amorphous alloys containing nanoscale crystalline particles. The appropriate selection of solute elements that can keep good ductile nature in the partially crystallized state is concluded to be the origin for the improvement of tensile strength even in the partially crystallized Fe–metalloid alloy.

4.3. Precipitation of graphite for the amorphous-forming alloys

Amorphous alloys are ordinarily composed of multi-components with suitable negative heats of mixing and hence the crystallized structure consists of multiple phases containing compound phases. The crystallized phases in the Fe–metalloid base system consist of α-Fe, γ-Fe, Fe_3C, Fe_3B, Fe_3P, Fe_2B and Fe_3Si, etc. Little is known about the Fe-based amorphous alloys in which the crystallized structure is occupied by a large amount of graphite phase. This is because the precipitation of graphite is due to the weak bonding of C against Fe and other constituent elements and the weak bonding state cannot lead to the formation of the amorphous phase. The weak bonding among the constituent elements enables an easy atomic movement and hence the precipitation of crystalline phases cannot be suppressed even during rapid solidification. The addition of 1.6 at.% B leads to the precipitation of Fe_3C containing B and the increase in the formation tendency of the Fe_3C phase seems to enable the production of the amorphous alloy. However, the 1.6 at.% B is not high enough to suppress the precipitation of graphite in a fully annealed sample. The graphite phase is recognized for the Fe–C–Si–B alloys containing less than about 4 at.% B and the volume fraction of the graphite phase is strongly dependent on B content. The strong dependence on B content is related to the result that the amorphous-forming tendency is also strongly dependent on B content. The similar strong dependence implies that the B element plays a dominant role in the bonding behavior among the constituent elements (Fe, C and Si).

It is important to discuss the precipitation process of the graphite phase because there have been no data on the precipitation behavior of graphite from an amorphous phase. It was shown in Section 3.2 that the $Fe_{80.4}C_{13.7}Si_{4.3}B_{1.6}$ (at.%) amorphous alloy crystallizes through the process of $Am \rightarrow Am' + \alpha\text{-Fe} \rightarrow Am'' + \alpha\text{-Fe} + Fe_3C \rightarrow \alpha\text{-Fe} + Fe_3C \rightarrow \alpha\text{-Fe} + Fe_3C$ + graphite. In the present study, we did not have any evidence on the direct precipitation of the graphite phase from the amorphous phase. The graphite phase appears to precipitate from the mixed α-Fe and Fe_3C phases after the completion of the crystallization reaction. In order to precipitate directly the graphite phase from the amorphous phase, the carbon content (14 at.%) in the amorphous phase is too low to form directly the graphite phase with 100% C. A kind of enrichment mechanism of C is necessary for the formation of the graphite phase. The formation of Fe_3C can be regarded as a kind of enrichment mechanism of C from the amorphous phase containing about 14 at.% C. The Fe_3C is a metastable phase as compared with graphite and the further increase in annealing temperature decomposes the Fe_3C phase to α-Fe and graphite phases with lower free energy. The decomposition reaction is accelerated by Si, but the B addition is presumed to suppress the decomposition [23]. The suppression effect enables the coexistence of Fe_3C and graphite. The homogeneous dispersion of the graphite phase reflects the fine and homogeneous dispersion of Fe_3C phase that is a feature of the crystallized structure from the amorphous phase.

4.4. High strength and large elongation for the mixed phase alloys of α-Fe + Fe_3C + graphite

It has been reported in the JIS handbook that the commercial FC20 cast iron has tensile fracture strength of 200–300 MPa and elongation of nearly 0% [13]. The tensile strength and elongation of the present $Fe_{80.4}C_{13.7}Si_{4.3}B_{1.6}$ ribbon in the fully crystallized state are 1200–2000 MPa and 4–13%, respectively. The high tensile strength of 1530 MPa and the large elongation of 9% were also obtained for the Fe–C–Si–B alloy cylinder annealed for 3.6 ks at 1200 K. The formation of the mixed structure for the Fe–C–Si alloys containing a small amount of B is useful for the remarkable improvement of mechanical properties. It was shown in Fig. 5 that the grain sizes are as small as 0.5 μm for α-Fe, 0.3 μm for Fe_3C and 1 μm for graphite which are much smaller than those (100 μm for α-Fe and 10 μm in width × 200 μm in length for flaky graphite) [24] for commercial FC20 cast iron. Consequently, the significant increases in strength and elongation are due to the refinement of the mixed structure. The preferential generation of cracks in the graphite region is subdivided by the homogeneous dispersion of fine graphite particles. In addition, the deformation of the α-Fe phase is also suppressed by the homogeneous dispersion of fine Fe_3C particles. Furthermore, since no boride is

formed in the 1.6 at.% B-containing alloy, the additional B is mainly dissolved into Fe_3C phase. The increase in the hardness of the Fe_3C phase by the dissolution of B [25] seems to cause a more effective dispersion strengthening.

5. SUMMARY

With the aim of developing a new high-strength and high-ductility alloy containing graphite particles, we examined the change in the as-quenched and annealed structures of the commercial FC20 cast iron by the addition of small amounts of B. The selection of B is due to the application of the three empirical rules for the achievement of high glass-forming ability to the cast iron consisting of the Fe–C–Si system. The results obtained are summarized as follows:

1. The melt-spun FC20 alloy consists of α-Fe, γ-Fe and Fe_3C phases, but the structure changes to a mixture of amorphous + α-Fe for the FC20 alloy containing 0.3 mass% B and to an amorphous phase for the FC20 alloy containing more than 0.4 mass% B.
2. The amorphous alloys have good bending ductility and exhibit high tensile strength of 3400 MPa for the 0.4 mass% B-containing alloy. The tensile strength increases further to 3800 MPa by the precipitation of nanoscale α-Fe particles into the amorphous phase after low-temperature annealing.
3. The crystallization of the FC20 alloy containing 0.4 mass% B takes place through the process of $Am \rightarrow Am' + \alpha\text{-Fe} \rightarrow Am'' + \alpha\text{-Fe} + Fe_3C \rightarrow \alpha\text{-Fe} + Fe_3C \rightarrow \alpha\text{-Fe} + Fe_3C$ + graphite. The crystalline phases obtained by annealing for 900 s at 1200 K have fine grain sizes of above 0.5 μm for α-Fe, 0.3 μm for Fe_3C and 0.5–1.5 μm for graphite. The graphite phase appears to have a nearly spherical morphology and the interparticle spacing is 0.5–2 μm. The precipitation of graphite occurs after the completion to α-Fe + Fe_3C and the formation of the enrichment phase (Fe_3C) of carbon seems to be essential for the formation of graphite after crystallization of the amorphous phase.
4. The crystallized alloys exhibit good mechanical properties of high tensile strength of 1200–2000 MPa and large elongation of 4–13% depending on annealing temperature. The fracture surface shows a typical dimple pattern.
5. A mostly single amorphous phase is also formed for cylindrical FC20 + 0.4% B alloys with a diameter of 0.5 mm and the annealed cylindrical alloy shows nearly the same tensile strength, hardness and large elongation as those for the melt-spun ribbon alloy. The findings that the new structure alloys consisting of amorphous + α-Fe and α-Fe + Fe_3C + graphite are formed by partial and full crystallization of the new amorphous alloys with compositions of FC20 + B indicate a new direction for the future development of high-strength Fe-based alloys.

Acknowledgements—This work is partly supported by the Inoue Superliquid Glass Project of Exploratory Research for Advanced Technology, Japan Science and Technology Corporation (JST).

REFERENCES

1. Masumoto, T. and Maddin, R., *Mater. Sci. Engng*, 1975, **19**, 1.
2. Chen, H. S., *Rep. Prog. Phys.*, 1980, **43**, 353.
3. Inoue, A., *Mater. Trans., Japan Inst. Metals*, 1995, **36**, 866.
4. Inoue, A. and Masumoto, T., US Patent No. 5032196; Japanese Patent 07-122120.
5. Peker, A. and Johnson, W. L., *Appl. Phys. Lett.*, 1993, **63**, 2342.
6. Zhang, T. and Inoue, A., *Mater. Trans., Japan Inst. Metals*, 1998, **39**, 857.
7. Inoue, A. and Gook, J. S., *Mater. Trans., Japan Inst. Metals*, 1995, **36**, 1180.
8. Inoue, A., Shinohara, Y. and Gook, J. S., *Mater. Trans., Japan Inst. Metals*, 1995, **36**, 1427.
9. Inoue, A., Zhang, T., Itoi, T. and Takeuchi, A., *Mater. Trans., Japan Inst. Metals*, 1997, **38**, 359.
10. Inoue, A., Zhang, T. and Takeuchi, A., *Appl. Phys. Lett.*, 1997, **71**, 464.
11. Chen, H. S. and Polk, D. E., *J. Non-Cryst. Solids*, 1974, **15**, 174.
12. Inoue, A., Masumoto, T. and Kimura, H. M., *J. Japan Inst. Metals*, 1978, **42**, 353.
13. ed. Japan Inst. Metals. *Metals Databook*. Maruzen, Tokyo, 1983.
14. Masumoto, T. (ed.), *Materials Science of Amorphous Alloys*. Ohmu, Tokyo, 1982, p. 281.
15. Shingu, P. H., Chudo, M. and Ozaki, R., *Suppl. Sci. Rep. Res. Inst. Tohoku Univ.*, 1980, **15**, 85.
16. Inoue, A., Komuro, M. and Masumoto, T., *J. Mater. Sci.*, 1984, **19**, 4125.
17. Inoue, A., *Bulk Amorphous Alloys*. Trans. Tech. Publishers, Zurich, 1998.
18. Powder Diffraction File Sets 19-20, JCPDS International Centre for Diffraction Data, 1979, p.196.
19. Inoue, A., in *Rare Earths*, Vol. 24, ed. K. A. Gschneidner Jr and L. Eyring. North-Holland, Amsterdam, 1997, p. 83.
20. Fan, C. and Inoue, A., *Mater. Trans., Japan Inst. Metals*, 1997, **38**, 1040.
21. Machlin, E. S., in *Thermodynamics and Kinetics*. Giro Press, New York, 1991, p. 125.
22. Pampillo, C. A. and Chen, H. S., *Mater. Sci. Engng*, 1974, **13**, 181.
23. Nicholson, M. E., *Trans. metall. Soc. A.I.M.E.*, 1957, **209**, 1.
24. Sato, T. (ed.), *Optical Micrographs and Explanation of Iron and Steels*. Maruzen, Tokyo, 1968, p. 230.
25. Sato, T., Nishizawa, T. and Ishihara, Y., *J. Japan Inst. Metals*, 1959, **23**, 403.